

USING WAVELET DENOISING AND MATHEMATICAL MORPHOLOGY IN THE SEGMENTATION TECHNIQUE APPLIED TO BLOOD CELLS IMAGES

MACARENA BOIX AND BEGOÑA CANTÓ

Universitat Politècnica de València
Plaza Ferrándiz y Carbonell, n.2, Alcoy (Alicante), 03801, Spain

(Communicated by Qing Nie)

ABSTRACT. Accurate image segmentation is used in medical diagnosis since this technique is a noninvasive pre-processing step for biomedical treatment. In this work we present an efficient segmentation method for medical image analysis. In particular, with this method blood cells can be segmented. For that, we combine the wavelet transform with morphological operations. Moreover, the wavelet thresholding technique is used to eliminate the noise and prepare the image for suitable segmentation. In wavelet denoising we determine the best wavelet that shows a segmentation with the largest area in the cell. We study different wavelet families and we conclude that the wavelet db1 is the best and it can serve for posterior works on blood pathologies. The proposed method generates goods results when it is applied on several images. Finally, the proposed algorithm made in MatLab environment is verified for a selected blood cells.

It is well-known that the image segmentation is a technique widely employed in applications such that image retrieval [3], object detection [14], [25] and medical image [9].

The increase of the capacity of the imaging devices makes it necessary to use accurate segmentation tools in medical applications. Furthermore, it is very difficult to visualize structures in complex three-dimensional image without deleting large portions where the data may be important. Tools, such as segmentation, can aid the medical staff in browsing through such large images by highlighting objects of particular importance. In addition, the segmentation can model the organs, tumors, and other structures for further analysis, quantification or simulation, see for example [8].

Image segmentation is to partition an image into meaningful parts, which generally consist of an object and a background. The segmentation technique is the first step in the image analysis and is the process of partitioning image pixels connected subsets, called regions, on the basis of homogeneity criteria. That is, with the segmentation technique, an image is separated into disjoint regions which union is the full image.

Several algorithms have been proposed in the literature to segment an image and they differ considerably in performance, expense of implementation and speed. The

2010 *Mathematics Subject Classification.* Primary: 68U10; Secondary: 65K05.

Key words and phrases. Blood cells images, segmentation, wavelet denoising, morphological operations.

selection of a suitable algorithm 1.00,0.50,1.00 depends on the type of the images and applications. Several mathematical models have been proposed to segment images, such as those cited in [24].

In the recent years, segmentation technique is used to extract useful information on medical images. This technique is a noninvasive pre-processing step for biomedical treatment. Cell classification has high interest for laboratories. For example, blood cell segmentation is used to study the diagnosis, treatment planning or locate tumors and other pathologies [5]. The segmentation of blood cell images is an important step for automatic cell analysis, because their final classification depends on the correct use of this technique.

There are several researches that study the segmentation technique. For example, an iterative approach based on circular histogram used to detect white blood is given in [22]. An approach for color image segmentation using entropy to determine the threshold is discussed in [12]. Segmentation method of red blood cell using different algorithms based in grey level thresholding, image gradient method and morphological operators is developed in [10]. In [20] segmentation and online learning algorithms in acquiring, tracking and analyzing cell-cycle behaviors of a population of cell generated by time-lapse microscopy are presented. A new variational model for image segmentation based on the complex GinzburgLandau model and a semi-norm defined by the authors is given [23]. In [2] the image segmentation algorithm makes use of an efficient connected components algorithm based on a novel approach for parallel merging. In [21] is shown the parallel edge-region-based segmentation algorithm targeted at reconfigurable MultiRing network. Finally, in [11] is combined two techniques for WBC segmentation, scale-space filtering and watershed clustering, to extract nucleus and cytoplasm respectively.

This paper is on segmentation technique used in blood cells with some diseases. White blood cells (leukocytes) are an important part of the body's defense against infectious organisms and foreign substances. To defend the body adequately, a sufficient number of white blood cells must receive a message that an infectious organism or foreign substance has invaded the body, get to where they are needed, and then kill and digest the harmful organism or substance. Some diseases can be detected by analyzing the white blood cells. For example, leukemia is a cancer of blood characterized an abnormal increase of white blood cells; liver disease describes a single number of diseases affecting the liver, since in this case the bilirubin increase and the red blood cells dead. Is these cases cells with this disease have an specific structure and we can segmented this in order to label the disease cells.

Some papers are refereed to image segmentation for blood cells. For example, in [4] the combination between region merging and watershed method is used, and in [1] methods of median filter and mathematical morphology operations are combined. In these papers they segment all the objects that are in the image.

The aim of this paper is to segment blood cell images to obtain the desired cells. That is, we only segment a cell(s) of study, and this is the difference with the above methods. For that, we show a modified method of the segmentation technique to improve the results desired. In this method, we integrate the wavelet transform to eliminate the noise. Also, we use morphological operations that allow us to improve the segmentation technique for blood cell images.

We applied this method to 30 images of blood cells. And the experiment shows that this method can obtain the boundary of the desired part of the biomedical images quickly and reliably. It has practical value in the biomedical image analysis.

1. **Theoretical framework.** In this section we show the theoretical framework used along this paper.

1.1. **Image segmentation.** A digital binary image (binary image) is a representation of a two-dimensional image where each pixel has only two possible values, 0 and 1. Usually the value for the object(s) in the image is 1 while the background takes the value 0.

Two pixels are neighbors if they share a common side or a common corner. A path is a sequence of pixels p_1, p_2, \dots, p_n such that p_k is a neighbor of p_{k+1} , for $k = 1, 2, \dots, n - 1$. We can define three types of neighborhoods of a pixel p :

- The 4-neighborhood of a pixel, $N_4(p)$, is the set that includes its horizontal and vertical neighbors.
- The 4-diagonal-neighborhood of a pixel, $N_D(p)$, is a set that includes its four diagonal neighbors.
- The 8-neighborhood of a pixel, $N_8(p)$, is a superset of the 4-neighborhood and contains the horizontal, vertical and diagonal neighbors.

Connectivity describes a relation between two or more pixels. With this property we can know if two pixels are part of the same object. A collection of pixels are connected if for any two pixels in the collection there exists a path of pixels in the collection such that one is the initial pixel and the other is the final pixel of the path.

From this, we can infer the definition for 4-connectivity and 8-connectivity. Two pixels p and q , both having values from a set V , are 4-connected if $q \in N_4(p)$ and 8-connected if $q \in N_8(p)$ (see figure 1).

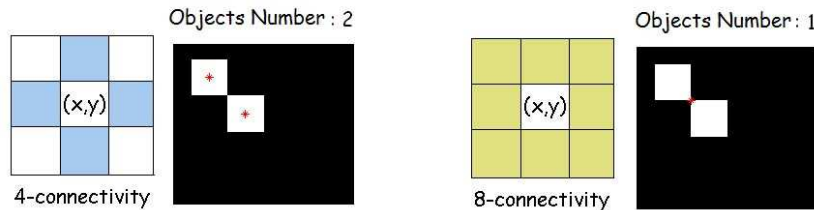


FIGURE 1. Illustration of (left) 4-connectivity, (right) 8-connectivity.

A connected set of pixels is usually called a region or connected components. To obtain a segmented image it is necessary to find all the regions of this image. For example, if in the figure 1 we consider 4-connectivity and there are two objects but if we consider 8-connectivity there is one object.

Image segmentation is the partitioning of the image I into nonoverlapping regions according to some common features. Segment is to determine connected sets $S_i \subset I$ whose union is the full image, that is

$$I = \bigcup_{i=1}^n S_i \quad / \quad S_i \cap S_j = \emptyset \quad i \neq j.$$

1.2. **Fundamental operations.** In this subsection we introduce the fundamental morphological operations.

Give an image (a subset) A in \mathbb{Z}^2 ,

- a) A complement of A , denoted by A^C , is given by $A^C = \{z / z \notin A\}$.
- b) The reflection of A , denoted by A^R , is $A^R = \{-a / a \in A\}$.
- c) The translation of A by the vector z , denoted by $(A)_z$, is defined by $(A)_z = \{b / b = a + z, a \in A\}$.

It is well-known that the morphological operations are used to image segmentation. The two most basic operations in mathematical morphology are erosion and dilation. Give the images (subsets) A and B in \mathbb{Z}^2 ,

- a) The basic effect of the erosion operator on a binary image is to erode away the boundaries of regions of the foreground pixels. The erosion of A by B , $A \ominus B$, is given by $A \ominus B = \{z / (B)_z \cap A \neq \emptyset\}$.
- b) The basic effect of the dilation operator on a binary image is to gradually enlarge the boundaries of regions of foreground pixels. The dilation of A by B , denoted by $A \oplus B$ is defined by $A \oplus B = \{z / (B^R)_z \cap A \neq \emptyset\}$.

With the dilation related pixels can be joined; with the erosion small objects or irrelevant details can be eliminated. In a binary image, the background's value is 0 and the value of the object is 1. Dilation in this case makes that the background pixels that are neighbors to pixels of the object take the value 1, that is, dilation enlarges the size of the objects. On the other hand, erosion in this case makes that the object pixels that are neighbors to pixels of the background take the value 0, that is, erosion decreases the size of the objects.

An issue often addressed in the image processing is the filling of a determined region by a given simple closed curve. This technique is based in dilation and complement operators (see [19] for more information). We start at a point p that is inside the border. This point has the value 1 and the background has the value 0 and we want to fill completely the specified region by p with 1's. If I is the image and B is the corresponding kernel, the process is given by

$$\begin{aligned}
 X_0 &= p \\
 X_1 &= (X_0 \oplus B) \cap I^C \\
 X_2 &= (X_1 \oplus B) \cap I^C \\
 X_3 &= (X_2 \oplus B) \cap I^C \\
 \dots &\dots\dots\dots \\
 X_n &= (X_{n-1} \oplus B) \cap I^C \quad n = 1, 2, 3, \dots
 \end{aligned}$$

The process of filling of a region is shown in figure 2.

1.3. Wavelet analysis. The algorithm proposed in this paper is based in wavelet analysis. This technique is used in different applications [13], and we use it to remove the noise of an image while the characteristics of this image are preserved. Wavelet analysis has been widely used (for more information see [15, 16, 17, 18]).

To preserve the desired characteristics it is important to choose an adequate threshold, T . There are two kinds of thresholds: the hard and the soft. The hard threshold signal is x , if $|x| > T$ and 0 if $|x| \leq T$, and the soft threshold signal is $\text{sign}(x)(|x| - T)$, if $|x| > T$ and 0 if $|x| \leq T$. Soft threshold is an extension of hard one, since it makes 0 the entries whose absolute value is lower that the threshold and it shrinks the nonzero coefficients towards 0 (see figure 3).

Using the threshold method it is further possible to reject noise and to enlarge signal to noise ratio. The denoised algorithm assumes that the signal contains low

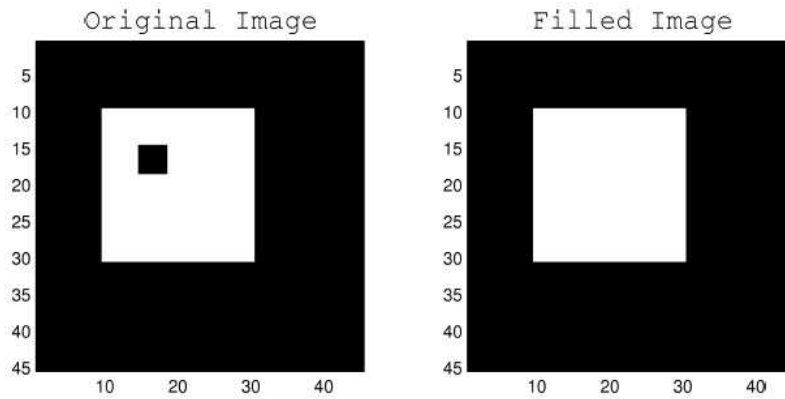


FIGURE 2. (Left) original image, (right) filled region.

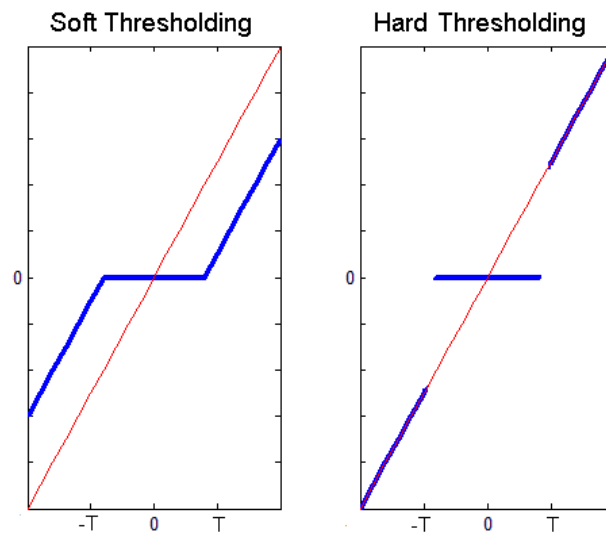


FIGURE 3. Transfer functions of the Soft and Hard Thresholding.

frequency components and it is corrupted by the additive noise where its power is lower than the power of the analyzed signal. The two-dimensional denoising procedure involves three steps:

- a) The signal decomposition, using a chosen wavelet function up to the selected level and evaluation of wavelet transform coefficients.
- b) The choice of threshold limits for each decomposition level and the modification of its coefficients.
- c) The signal reconstruction from modified wavelet transform coefficients.

The results of this process depend on the proper choice of the wavelet functions and the selection of the threshold limits. The process to apply wavelet analysis is as follows: Firstly, the optimal threshold is selected. When the grey value of a

pixel is greater than the threshold, the pixel belongs to the interested region and its color is white. Conversely, if the grey value of a pixel is lower than the threshold, the pixel belongs to the background and its color is black. Next, the best level of decomposition is selected. For that, an image and a wavelet family are taken and the results are compared using different levels of decomposition. Hence, the best level in the analysis is chosen. Finally, the best wavelet family for this level is chosen. The different wavelet families make different trade-offs between how compactly the basis functions are localized in the space and how smooth they are. So, the election of the wavelet family depends on the desired results.

2. Methodology. In the present study we use the images of two databases to apply the proposed method: the images of the UAB Pathology Department PEIR Digital Library (denoted by P) and the images of the Medeiros' collection (denoted by M) re. These databases are selected because they include a variety of cases.

In this section we present a method to isolate the diseased cells of the blood in order to label them. We use the MatLab software and, for this reason, the image needs to be processed as follows (figure 4 is a flowchart that represents the segmentation process).

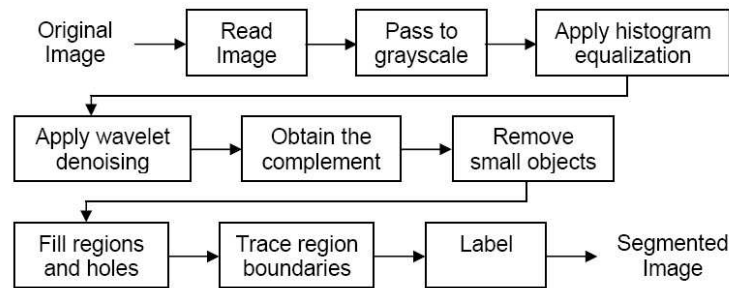


FIGURE 4. Segmentation process.

Moreover, in Matlab environment we have developed an interface to help the user. This interface is self-contained and shows the segmentation of blood cells images step by step (see figure 5 as an example of the interface).

After reading the image, its size is increased 3 times to get a better display. Then, the segmentation process is as follows:

- a) Transform the color image to grey image.

The color image, namely RGB (Red, Green and Blue) is read in MatLab environment and it is stored as a matrix with $m \times n \times 3$ bytes. The stored image is transformed to grey image. Grey image, which has only brightness information, is expressed by a matrix with $m \times n$ bytes. We take a pixel and for each component R, G and B we apply the following equation,

$$\text{Grey} = 0.289R + 0.5870G + 0.1140B.$$

- b) Improve the contrast of the images.

The histogram equalization improves the contrast of images. The histogram is an important tool in the processing of an image, because it can show their characteristics and defects. The histogram is a graphical distribution of the grey levels of pixels in a digital image. It provides a simple representation of

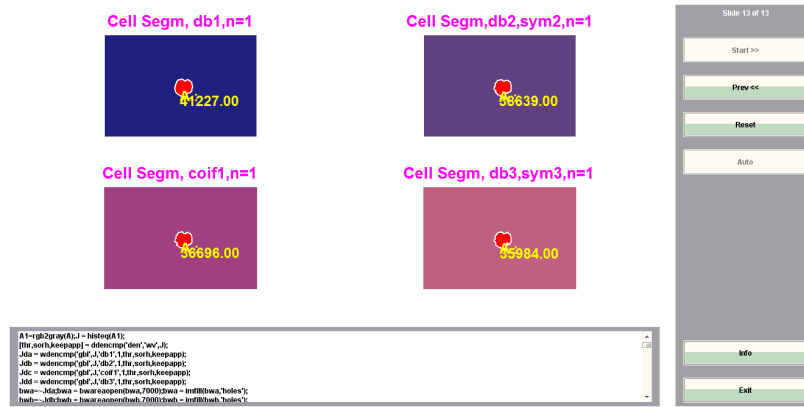


FIGURE 5. Comparison of different wavelets.

the concentration versus brightness of pixels in an image. Watching him, we know if an image is dark or light and if it has high or low contrast.

The process of adjust the intensity values can be done automatically by a function that performs the histogram equalization. This function involves the change of the intensity values so that the histogram of the output image approximately matches an specified histogram.

c) Wavelet-packet denoising.

Wavelet denoising attempts to remove the noise in the image while preserves the image characteristics. We apply the universal threshold given by $\sigma \left(\sqrt{2 \log(m \times n)} \right)$, where σ is the variance of the estimated noise and $m \times n$ is the number of pixels in the image. We use a soft threshold because it has some advantages, for example, it makes algorithms mathematically more tractable (see [6], [7] for more information).

On wavelet families, we study Daubechies (dbN), $N = 1, 2, 3$, Coiflets (coifN), $N = 1, 2, 3$, and Symlets (symN), $N = 2, 3$, where N is the order. We choose these families because they share some characteristics such as orthogonality, biorthogonality, compact support, a large number of zero moments and we can make their analysis using the Discrete Wavelet Transform or using the Continuous Wavelet Transform.

The process is as follows:

- We apply different wavelets on the same image to choose the best level of the decomposition.
- With the level fixed we compare the measurements obtained for some images using the wavelet families previously selected.
- We choose the wavelet that shows the best results. In our paper we compare the area and the perimeter, but we can make the analysis using another parameters.

Note that in the process, we do not apply the binarization because the images are already binarized using this wavelet denoising.

d) Fundamental operations.

The complement of the image is obtained. That is, the difference between each value and the value of the maximum pixel is used in the output image. In this

case, the dark areas become lighter and vice versa. In the output image, the objects take the value 1 (white) and the background takes the value 0 (black).

The obtained binary image has holes. A hole is a set of background pixels that are not filled from the edge of the image. To fill the holes we use the filling operator. In this case, we do not use the dilation operator because we want to fill certain areas (subsets) and not all the set.

e) Remove small objects.

We remove small objects using a morphological technique. In this case, the method removes all the objects which have less than 750 pixels. This number is determined by the user of the application.

f) Segmented image.

Finally, the algorithm traces region boundaries in the image and label the image for later use. Thus, the image is segmented and we can obtain some characteristics such that its area and perimeter.

We apply the proposed method to original images. This method is represented, for a particular image in figure 6.

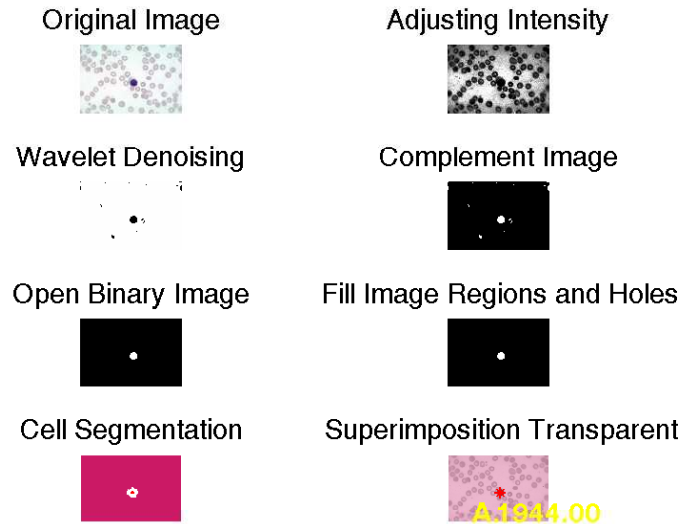


FIGURE 6. Segmentation of a blood cell image that contains a small lymphocyte.

3. Results and discussion. In accordance with the proposed method, the best level in wavelet denoising is $n = 1$. We apply the above methodology to a set of images provided by the two databases P and M. This methodology has been implemented in MatLab software.

Figures 7 and 8 show examples of the segmentation when there exist more than one cell to segment. In the first figure we use the wavelet ‘coif3’ and in the second figure we use the wavelet ‘sym3’, both of them at level $n = 1$. We can observe that the segmentation is accurate in both cases and our algorithm finds all the objects.

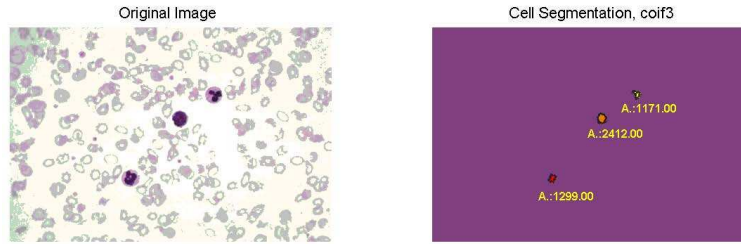


FIGURE 7. Image P510. Segmentation of a blood cell image that contains schistocytes (micro blood film neutrophils and lymphocyte).

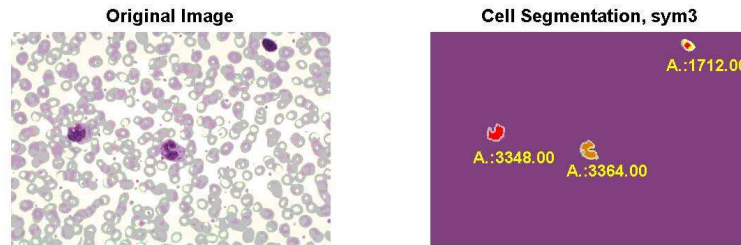


FIGURE 8. Image P569. Segmentation of a blood cell image that contains toxic granulation (micro blood film with band and metamyelocyte).

If we study all the cases, we can conclude that the accuracy of the segmentation depends strongly on which wavelet is chosen. If we apply different wavelets in the same image at level $n = 1$, we observe that the area and perimeter of the segmented section are different and depends on the wavelet used. We show this fact in the following table.

| n=1 | Area M23 | Perim. M23 | Area M21 | Perim. M21 | Area P1816 | Perim. P1816 | Area P2723 | Perim. P2723 |
|-------|-------------|---------------|-------------|---------------|---------------|-----------------|---------------|-----------------|
| db1 | 16223 | 495 | 12939 | 638 | 18413 | 569 | 41227 | 846 |
| db2 | 14954 | 726 | 11463 | 734 | 17043 | 777 | 38639 | 1217 |
| db3 | 13480 | 669 | 10131 | 683 | 15673 | 671 | 35984 | 1252 |
| coif1 | 13703 | 761 | 10306 | 761 | 15956 | 759 | 36696 | 1149 |
| coif2 | 10610 | 852 | 7074 | 821.5 | 12589 | 860 | 18039 | 1557 |
| coif3 | 7979 | 923.7 | 4353 | 862.1 | 9432 | 756 | 8150 | 1568 |
| sym2 | 14954 | 726 | 11463 | 734 | 17043 | 777 | 38639 | 1217 |
| sym3 | 13480 | 669 | 10131 | 683 | 15673 | 671 | 35984 | 1252 |

TABLE 1. Comparison of different wavelets applied to some blood cells images in terms of the area and the perimeter. The rest of images are in the Annex.

In figure 5, for example, we can see the difference over the area and the perimeter. And we can observe in this figure that with the 'db2' and 'sym2' wavelets we obtain the same results. The same happens with the 'db3' and 'sym3' wavelets.

Moreover, if we study the table, we conclude that the best results for the area of these images are obtained with the ‘db1’ wavelet and the level of decomposition $n = 1$.

In figures 9, 10 and 11 we represent some of the obtained results in the table. In this way, we can see in a visual way that the results of the table are correct. Moreover, we can observe that the segmentation with the ‘db1’ wavelet and the level of decomposition $n = 1$ is the most accurate.

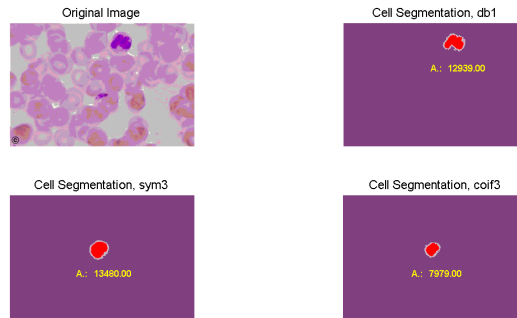


FIGURE 9. Image M21. Segmentation of a blood cell image that contains parasites and fungus.



FIGURE 10. Image M23. Segmentation of a blood cell image that contains a lymphocyte.

4. Conclusions. In this paper, we have developed an algorithm based on MatLab software that aims to segment blood cell images. This algorithm is completely automated, fast, accurate and requiring rather modest computing. It can show isolated cells and we can obtain the area and perimeter of them. It has been tested on a total of 30 images from two sources with a high success rate.

The algorithm combines the automatic threshold selection with the use of morphological operations to segment blood cell images and we obtain an excellent result.

Using this algorithm the best results for the processed images have been obtained with the wavelet ‘db1’ and the level of decomposition $n = 1$.

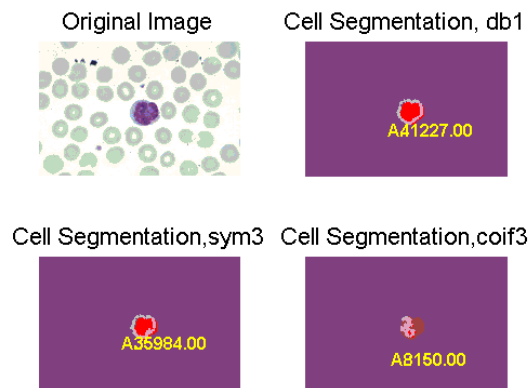


FIGURE 11. Image P2723. Segmentation of a blood cell image that contains metamyelocyte (micro wright stained blood film case of streptococcal sepsis cell).

The described method in this paper is sufficient for the correct detection and segmentation of nucleated cells. Thus, the isolated cells, that they are diagnostically important, have been detected and correctly segmented.

Acknowledgments. The authors wish to thank Dr. Nivaldo Medeiros and the UAB Pathology Department PEIR Digital Library (Dr. Peter G. Anderson) since they are the source of all images and the commentaries of them in this paper.

Annex. The lines indicates that the wavelet does not detect the cell.

| | | | | | | | | |
|------|-------------------|------------------|------------------|-------------------|---------|--------|------------------|------------------|
| M1 | db1 | db2 | db3 | coif1 | coif2 | coif3 | sym2 | sym3 |
| Area | 8300 9662 | 5409 5741 | 1300 1654 | 3344 2154 | - - | - - | 5409 5741 | 1300 1654 |
| Per. | 1056.3 1262.4 | 1262.4 1641.7 | 598.60 505.35 | 1240.88 763.31 | - - | - - | 1262.4 1641.7 | 598.60 505.35 |
| M10 | | | | | | | | |
| Area | 17140 | 10123 | 6094 | 6349 | 2419 | - | 10123 | 6094 |
| Per. | 1494.4 | 1512.1 | 911.3 | 976.98 | 461.10 | - | 1512.1 | 911.3 |
| M22 | | | | | | | | |
| Area | 12845 2501 | 1837.96 - | 3032 - | 3233 -4 | - - | - - | 8794 - | 3032 - |
| Per. | 1454.15 420.92 | 1262.4 - | 740.54 - | 795.44 - | - - | - - | 1837.96 - | 740.54 - |
| M35 | | | | | | | | |
| Area | 17741 | 13502 | 10355 | 10547 | 6052 | 3112 | 13502 | 10355 |
| Per. | 1401.4 | 1375.9 | 726.58 | 768.99 | 1030.17 | 756.35 | 1375.9 | 726.58 |
| M58 | | | | | | | | |
| Area | 12114 4462 | 10101 - | 5421 - | 6236 - | - - | - - | 10101 - | 5421 - |
| Per. | 744.48 925.3 | 1020.41 - | 1279.69 - | 1394.18 - | - - | - - | 1020.41 - | 1279.69 - |
| M205 | | | | | | | | |
| Area | 21084 | 13552 | 5244 | 5244 | 1228 | - | 13552 | 5244 |
| Per. | 1043 | 1475 | 559.7 | 559.7 | 163.80 | - | 1475 | 559.7 |
| M209 | | | | | | | | |
| Area | 3120 2684 | 1420 - | - - | - - | - - | - - | 1420 - | - - |
| Per. | 368.27 461.14 | 299.5 - | - - | - - | - - | - - | 299.5 - | - - |

TABLE 2. Mendeiros' images.

| | | | | | | | | |
|-----------|--------|--------|--------|--------|--------|--------|--------|--------|
| P2726 | db1 | db2 | db3 | coif1 | coif2 | coif3 | sym2 | sym3 |
| Area | 47385 | 44588 | 29350 | 33281 | 5251 | - | 44588 | 29350 |
| Perimeter | 985 | 1452 | 3167 | 2662 | 902.2 | - | 1452 | 3167 |
| P505 | | | | | | | | |
| Area | 10649 | 8423 | 6308 | 6450 | 3495 | 1147 | 8423 | 6308 |
| Perimeter | 696 | 771.2 | 603.5 | 623 | 668.04 | 547.85 | 771.2 | 603.5 |
| P506 | | | | | | | | |
| Area | 11638 | 10524 | 9300 | 9490 | 6879 | 4555 | 10524 | 9300 |
| | 8724 | 6946 | 5951 | 6078 | 3401 | 1500 | 6946 | 5951 |
| Perimeter | 501.1 | 518.27 | 487.89 | 504.9 | 637.70 | 487.57 | 518.27 | 487.89 |
| | 455.65 | 575.69 | 546.48 | 606.93 | 673.11 | 533.37 | 575.69 | 546.48 |
| P507 | | | | | | | | |
| Area | 3459 | 2769 | 2233 | 2313 | 1153 | - | 2769 | 2233 |
| Perimeter | 298.35 | 297.18 | 311.32 | 304.29 | 318.33 | - | 297.18 | 311.32 |
| P508 | | | | | | | | |
| Area | 10229 | 9135 | 6978 | 7891 | 2812 | - | 9135 | 6978 |
| | 8412 | 7144 | 6139 | 6353 | 2778 | - | 7144 | 6139 |
| Perimeter | 418.19 | 555.97 | 510.5 | 577.03 | 709.74 | - | 555.97 | 510.5 |
| | 430.1 | 565.6 | 796.87 | 645.41 | 796.65 | - | 565.6 | 796.87 |
| P510 | | | | | | | | |
| Area | 7362 | 5816 | 4776 | 4919 | 2791 | 1171 | 5816 | 4776 |
| | 7467 | 6658 | 5840 | 6050 | 4015 | 2412 | 6658 | 5840 |
| | 6166 | 5120 | 4381 | 4465 | 2674 | 1299 | 5120 | 4381 |
| Perimeter | 414.68 | 620.01 | 530.07 | 557.09 | 485.39 | 362.96 | 620.01 | 530.07 |
| | 340.74 | 468.33 | 409.95 | 450.76 | 428.76 | 454.84 | 468.33 | 409.95 |
| | 387.81 | 410.29 | 403.85 | 421.10 | 385.55 | 359.55 | 410.29 | 403.85 |
| P513 | | | | | | | | |
| Area | 15280 | 13032 | 11592 | 11592 | 8300 | 4392 | 13032 | 11592 |
| Perimeter | 933 | 690 | 586 | 586 | 445.5 | 475.4 | 690 | 586 |
| P521 | | | | | | | | |
| Area | 7495 | 6259 | 4989 | 5192 | 2208 | - | 6259 | 4989 |
| | 7281 | 6472 | 5679 | 5781 | 3620 | 1775 | 6472 | 5679 |
| Perimeter | 503.97 | 683.47 | 646.64 | 679.98 | 765.68 | - | 683.47 | 646.64 |
| | 419.28 | 508.39 | 496.88 | 536.76 | 584.01 | 467.39 | 508.39 | 496.88 |
| P522 | | | | | | | | |
| Area | 6496 | 5060 | 3788 | 3788 | - | - | 5060 | 3788 |
| | 7076 | 5688 | 4580 | 4580 | 1676 | - | 5688 | 4580 |
| | 7276 | 6104 | 4996 | 4996 | 1520 | - | 6104 | 4996 |
| Perimeter | 671.07 | 610 | 513.73 | 513.73 | - | - | 610 | 513.73 |
| | 583.87 | 524.65 | 493.92 | 493.92 | 291.01 | - | 524.65 | 493.92 |
| | 552.55 | 514.89 | 493.24 | 493.24 | 236.08 | - | 514.89 | 493.24 |

TABLE 3. PEIR's images.

| | | | | | | | | |
|-----------|--------|--------|--------|--------|--------|--------|--------|--------|
| P569 | db1 | db2 | db3 | coif1 | coif2 | coif3 | sym2 | sym3 |
| Area | 5952 | 5232 | 4552 | 4552 | 2752 | 1312 | 5232 | 4552 |
| | 14024 | 11500 | 9196 | 9196 | 5276 | 2592 | 11500 | 9196 |
| | 12268 | 10616 | 9028 | 9028 | 5748 | 3372 | 10616 | 9028 |
| Perimeter | 331.20 | 315.20 | 293.54 | 293.54 | 239.88 | 174.91 | 315.20 | 293.54 |
| | 827.85 | 659.87 | 591.58 | 591.58 | 462.81 | 376.67 | 659.87 | 591.58 |
| | 773.42 | 693.72 | 425.15 | 425.15 | 416.57 | 296.77 | 693.72 | 425.15 |
| P580 | | | | | | | | |
| Area | 7609 | 5236 | 4436 | 4549 | 2606 | - | 5236 | 4436 |
| | 6046 | 6573 | 5744 | 5822 | 3848 | 2186 | 6573 | 5744 |
| Perimeter | 353.91 | 469.40 | 441.16 | 471.49 | 433.83 | - | 469.40 | 441.16 |
| | 416.43 | 495.55 | 519.39 | 503.29 | 499.29 | 379.10 | 495.55 | 519.39 |
| P583 | | | | | | | | |
| Area | 9947 | 9068 | 8150 | 8299 | 6015 | 4018 | 9068 | 8150 |
| | 13538 | 12466 | 11376 | 11572 | 8804 | 6252 | 12466 | 11376 |
| Perimeter | 384.88 | 514.27 | 477.3 | 486.46 | 568.4 | 481.33 | 514.27 | 477.3 |
| | 454.62 | 592.3 | 595.04 | 633.75 | 676.04 | 626.77 | 592.3 | 595.04 |
| P985 | | | | | | | | |
| Area | 1784 | 1416 | 1080 | 1080 | - | - | 1416 | 1080 |
| | 8868 | 7808 | 6984 | 6984 | 4748 | 2892 | 7808 | 6984 |
| | 8924 | 8076 | 7264 | 7264 | 5060 | 3212 | 8076 | 7264 |
| Perimeter | 172.18 | 156.18 | 140.18 | 140.18 | - | - | 156.18 | 140.18 |
| | 397.34 | 378.51 | 359.68 | 359.68 | 302.61 | 243.30 | 378.51 | 359.68 |
| | 394.02 | 378.02 | 359.20 | 359.20 | 305.54 | 246.23 | 378.02 | 359.20 |
| P1812 | | | | | | | | |
| Area | 14608 | 12876 | 11364 | 11609 | 7960 | 4705 | 12876 | 11364 |
| Perimeter | 707.81 | 797.51 | 749.33 | 852.55 | 943.95 | 776 | 797.51 | 749.33 |
| P223740 | | | | | | | | |
| Area | 1804 | - | - | - | - | - | - | - |
| Perimeter | 479.99 | - | - | - | - | - | - | - |
| P223734 | | | | | | | | |
| Area | 1265 | - | - | - | - | - | - | - |
| Perimeter | 396.29 | - | - | - | - | - | - | - |
| P214010 | | | | | | | | |
| Area | 1220 | - | - | - | - | - | - | - |
| Perimeter | 320.11 | - | - | - | - | - | - | - |
| P213970 | | | | | | | | |
| Area | 1628 | - | - | - | - | - | - | - |
| Perimeter | 210.91 | - | - | - | - | - | - | - |
| P223719 | | | | | | | | |
| Area | 780 | - | - | - | - | - | - | - |
| Perimeter | 256.47 | - | - | - | - | - | - | - |

TABLE 4. PEIR's images.

REFERENCES

- [1] D. Anoraganingrum, *Cell segmentation with median filter and mathematical morphology operation*, in "International Conference on Image Analysis and Processing," **9** (1999), 183–188.
- [2] D. A. Bader, J. Jájá, D. Harwood and L. L. Davis, *Parallel algorithms for image enhancement and segmentation by region growing, with an experimental study*, Journal of Supercomputing, **10** (1996), 141–168.
- [3] C. C. Chiang, Y. P. Hung and G. C. Lee, *A learning state-space model for image retrieval*, IEEE. Trans. Mult., **10** (2008), 1–10.
- [4] H. Chan, J. Li-Jun and B. Jiang, *Wavelet transform and morphology image segmentation algorithm for blood cell*, in "Industrial Electronics and Applications" ICIEA 2009, 4th IEEE Conference (2009), 542–545.
- [5] L. Costrarido, "Medical Image Analysis Methods: Medical-image Processing and Analysis for CAD Systems," 2nd edition, Taylor and Francis, New York, 2005.
- [6] D. L. Donoho, *An ideal spatial adaptation by wavelet shrinkage*, Biometrika, **81** (1994), 425–455.
- [7] D. L. Donoho, *De-noising by soft thresholding*, IEEE. Trans. Inf. Theory, **41** (1995), 613–627.
- [8] F. Gibou, D. Levy, C. Cárdenas, P. Liu and A. Boyer, *Partial differential equations-based segmentation for radiotherapy treatment planning*, Mathematical Biosciences and Engineering, **2** (2005), 209–226.
- [9] V. Grau, A. U. Mewes, M. Alcáñiz, R. Kikinis and S. K. Warfield, *Improved watershed transform for medical image segmentation using prior information*, IEEE. Trans. Med. Imaging, **23** (2004), 447–458.
- [10] K. B. How, A. S. Kok Bin, N. T. Siong and K. K. Soo, *Red blood cell segmentation utilizing various image segmentation techniques*, in "Proceedings of International Conference on Man-Machine Systems," Malaysia, (2006).
- [11] K. Jiang, Qing-Min and S. Y. Dai, *A novel white blood cell segmentation scheme using scale-space filtering and watershed clustering*, in "Proceedings of The Second International Conference on Machine Learning and Cybernetics," Xian, (2003).
- [12] R. S. Kumar, A. Verma and J. Singh, *Color image segmentation and multi-level thresholding by maximization of conditional entropy*, Int. Sig. Processing, **3** (2006).
- [13] J. Liang, S. Elangovan and J. Devotta, *Application of wavelet transform in travelling wave protection*, Int. Elect. Pow. Energy, **22** (2000), 537–542.
- [14] D. Liu and T. Chen, *DISCOV: A framework for discovering objects in video*, Int. Trans. Multimedia, **10** (2008), 200–208.
- [15] S. Mallat, *Zero-crossings of a wavelet transform*, Int. Trans. Inf. Theory, **37** (1991), 1019–1033.
- [16] S. Mallat and W. L. Hwang, *Singularity detection and processing with wavelets*, Int. Trans. Inf. Theory, **38** (1992), 617–643.
- [17] S. Mallat and S. Zhong, *Characterization of signals from multiscale edges*, Int. Trans. Patt. Anal. Mac. Int., **14** (1992), 710–732.
- [18] B. Ninga, D. Qinyuna, H. Darena and F. Jib, *Image coding based on multiband wavelet and adaptive quad-tree partition*, Journal of Computational and Applied Mathematics, **195** (2006), 2–7.
- [19] P. Soille, "Morphological Image Analysis: Principles and Applications," 2nd edition, Springer-Verlag, New York, 1999.
- [20] M. Wang, X. Zhou, F. Li, J. Huckins, R. W. King and S. T. Wong, *Novel cell segmentation and online learning algorithms for cell phase identification in automated time-lapse microscopy*, in "Proceedings of Biomedical Imaging: From Nano to Macro 2007, ISBI 2007 4th IEEE International Symposium," (2007).
- [21] M. A. Wani, D. Zhang and H. Arabnia, *Parallel edge-region-based segmentation algorithm targeted at reconfigurable multiRing network*, Journal of Supercomputing, **25** (2003), 43–62.
- [22] J. Wu, P. Zeng, Y. Zhou and C. Olivier, *A novel color segmentation method and its application to white blood cell image analysis*, in "IEEE Proceeding, ICSP 2006", (2006).
- [23] Y. Zhai, D. Zhang, J. Sun and B. Wu, *A novel variational model for image segmentation*, Journal of Computational and Applied Mathematics, **235** (2011), 2234–2241.
- [24] J. Y. Zhou, X. Fang and K. Ghosh, *Multiresolution filtering with application to image segmentation*, Math. Comp. Model., **24** (1996), 177–195.

- [25] J. Y. Zhou, E. P. Ong and C. C. Ko, *Video object segmentation and tracking for content-based video coding*, in “Proceedings of IEEE International Conference on Multimedia and Expo, ICME 2000,” USA (2000).

Received April 17, 2012; Accepted October 03, 2012.

E-mail address: mboix@mat.upv.es

E-mail address: bcanto@mat.upv.es